

Journal of Materials Chemistry A

Accepted Manuscript



This is an *Accepted Manuscript*, which has been through the Royal Society of Chemistry peer review process and has been accepted for publication.

Accepted Manuscripts are published online shortly after acceptance, before technical editing, formatting and proof reading. Using this free service, authors can make their results available to the community, in citable form, before we publish the edited article. We will replace this *Accepted Manuscript* with the edited and formatted *Advance Article* as soon as it is available.

You can find more information about *Accepted Manuscripts* in the [Information for Authors](#).

Please note that technical editing may introduce minor changes to the text and/or graphics, which may alter content. The journal's standard [Terms & Conditions](#) and the [Ethical guidelines](#) still apply. In no event shall the Royal Society of Chemistry be held responsible for any errors or omissions in this *Accepted Manuscript* or any consequences arising from the use of any information it contains.

Reactive Adsorption of Mustard Gas Surrogate on Zirconium (Hydr)Oxide/Graphite Oxide Composites: The Role of Surface and Chemical Features

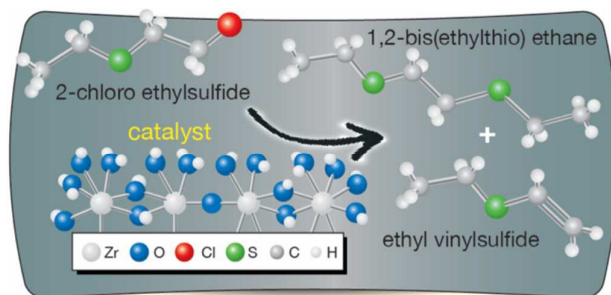
Dimitrios A. Giannakoudakis^{1,2}, Joshua K. Mitchell¹ and Teresa J. Bandosz^{1,2*}

¹ Department of Chemistry, The City College of New York, CUNY, 160 Convent Ave, New York, NY, 10031, USA

² The Graduate Center of the City University of New York, 365 Fifth Avenue, New York, NY, 10016, USA

*Corresponding author: E-mail: tbandosz@ccny.cuny.edu; Fax: +1 212 650 6107; Tel: +1 212 650 6017

Table of contents entry



Zirconium (hydr)oxide/Graphite oxide composites are efficient media for the selective detoxification of mustard gas surrogate, 2-Chloroethyl ethyl sulfide, at ambient conditions.

Key words: Zirconium hydroxide, Graphite Oxide composites, 2-chloroethyl ethyl sulfide, reactive adsorption, mustard gas, detoxification

Abstract

Zirconium (hydr)oxide and its composites with various amounts of graphite oxide (GO) were successfully synthesized using a controlled rate precipitation method. This economically feasible and a quick aqueous synthetic route, which is also suitable for large-scale production, leads to the amorphous materials of a complex texture, relatively large surface area, and high hydroxyl group density. Extensive surface characterization with various chemical and physical methods revealed significant differences in the surface features. The addition of the GO phase increased the surface chemical and structural heterogeneity. The composites were evaluated as reactive adsorbents of mustard gas surrogate, 2-Chloroethyl ethyl sulfide (CEES). They showed higher adsorption capacities than those measured on zirconium (hydr)oxide. The results indicated the paramount role of the porosity and surface chemistry in the reactive adsorption process. The GO addition enhances both these features by promoting a high dispersion of the inorganic phase around the carbonaceous phase. 5 % GO in the composites was found to be an optimum amount, since it increases the surface area and the number of terminal hydroxyl groups. While the former increased from 208 m²/g for pure zirconium (hydr)oxide to 269 m²/g for the best composite, for the latter a 141 % increase was noticed. Moreover, the maximum weight uptakes for zirconium (hydr)oxide and the composite with 5 % carbonaceous phase were 106 and 205 mg/g, respectively. Two general CEES adsorption pathways were proposed. The first one is the retention of organic molecules by physical forces, and the second - the catalytic and selective transformation of CEES to ethyl vinyl sulfide by dehydrohalogenation, and the transformation to 1,2-bis(ethylthio) ethane by polymerization.

Introduction

World War I brought one of the saddest realities in history: the vast scale usage of Chemical Warfare Agents (CWAs). Bis(2-chloroethyl) sulfide, formally known as mustard gas (HD), can be regarded as the King of battle gases since it has caused casualties, widespread panic, and terror incapacitating victims. Blistering, blindness, anemia, and shortness of breath were the most common symptoms. This alkylating agent vigorously erodes the epithelial tissue, which is followed by the release of HCl, which damages the respiratory, olfactory, and visual systems.¹ Considering its use and toxicity, it is of paramount importance to develop detoxification methods and materials that can efficiently eliminate (or absorb and decompose) this compound from the environment and the stockpiles, and also to be applied in active filtration systems.

Thermal decompositions and neutralization are the most common methods to destroy organic pollutants.^{1,2} Since decomposition by heat expends large amounts of energy and produces CO₂ and other toxic species, it is unfavorable and sometimes not practical. On the other hand, neutralization has drawbacks related to the usage of caustic compounds and the generation of liquid wastes. To surmount this, a development of new materials for a more efficient and safer detoxification or selective decomposition of CWAs has been a recent focus of researchers.

Metal (hydr)oxide based materials proved to work well as adsorbents of various gases. Beside their relatively high surface area, basic and acidic surface sites (Lewis and Brønsted-Lowery) were also found as important.³ Metal (hydr)oxides are known to strongly interact and adsorb a wide range of reactive toxic gases, specifically

compounds with sulfur^{4,5} and/or with chloride terminal groups.⁶

Zirconium oxide or zirconia is a well-studied ceramic, which composites have been widely investigated, due to their high thermal stability, hydroxyl group density, and relatively large surface area.^{5,7-9} These are essential features for the detoxification process based on adsorption. For adsorption applications amorphous zirconium hydroxide is preferred among the various lattices of zirconium oxides (monoclinic, orthorhombic, and cubic) because of its favorable surface features.¹⁰⁻¹² This material was reported as a good reactive adsorbent of sulfur containing toxic gases, such as SO₂ and H₂S, as well as for NH₃.^{5,11,13,14} Zirconium hydroxide, pure or impregnated with triethylenediamine, showed high adsorption performance towards removal of Cl₂, COCl₂ and HCl from streams of air.⁶ Zirconium has also been proved to play a key role in the degradation of CWAs as a dopant in Ti-Fe oxides⁷ or Titania,¹⁵ since it increases the surface area and the reactivity of the composites. Moreover, zirconium oxides play a catalytic role in the transformations of various organic molecules, especially for dehydration reactions.¹⁶

Since the surface chemistry and the dispersion of the active centers of zirconium hydroxide are important, accentuating those properties will significantly enhance target interactions. A formation of composites with graphite oxide (GO) is one of the ways to enhance zirconium hydroxide surface features. GO has been proven to notably increase the surface area and the number of active sites when used in composites with metal (hydr)oxides (such as iron¹⁷, zinc⁴ and copper¹⁸) MOFs,¹⁹⁻²¹ or even with organic compounds like porphyrinoids²² and chitosan.^{23,24} These composites have shown synergistic effects that generate unique physical and chemical

properties compared to their individual precursors. These new properties improved the material's adsorption capabilities for various toxic gases, including SO₂, NH₃ and H₂S as well as for chemical warfare surrogates²⁵⁻²⁹, by increasing the structural and chemical heterogeneity and the density of the active hydroxyl groups.

The research presented in this paper is based on a hypothesis that a composite of zirconium (hydr)oxide and GO exhibit a good performance toward the removal of HD surrogate, 2-chloroethyl ethyl sulfide (CEES), from air at ambient conditions. The latter contains a similar functional group (-SCH₂CH₂Cl) to the actual CWA-HD. To the best of our knowledge, no study has been done on the adsorption of chemical warfare agents from air using composites of zirconium hydroxide and a carbonaceous phase, such as graphite oxide. Therefore, such composites with various amounts of graphite oxide were synthesized and tested for the removal of CEES vapors from air at ambient conditions. The focus is on the role of the carbonaceous phase and on the features that have the most crucial contribution for the reactive adsorption. Based on this, the mechanism of reactive adsorption is proposed.

Results and discussion

X-ray diffraction powder (XRD) patterns of the materials tested are presented in Fig. S1 of Supplementary Information. Regardless the presence and amount of GO, all samples show a lack of crystallinity. The characteristic peak of graphite oxide at 11.7° 2 θ is not seen, indicating an exfoliation of GO within the amorphous structure of the zirconium hydroxide.

For adsorption applications, porosity is considered as one of the most important

features. The structural parameters calculated from measured nitrogen adsorption isotherms are presented in Fig. 1A, B and C. If the final product were a physical mixture, an increase in GO content would lead to a decreased porosity of the synthesized materials, since the surface area of GO is only $4 \text{ m}^2/\text{g}$ and its total pore volume is $0.002 \text{ cm}^3/\text{g}$.³⁰ The hypothetical surface areas and total pore volumes were calculated assuming a physical mixture of both components and that both components contribute to these parameters following their percentage in the composites. The comparison of the parameters of the porous structure is presented in Figures 1A and 1B. The synergistic effect of the composite formation on porosity development is clearly seen from the comparison of the measured and hypothetical values, where the most visible differences are those for ZrGO5 (+ 36 %) and ZrGO20 (+42%). The measured surface area of the former is 29 % higher than that of ZrOH. The increments for ZrGO1, ZrGO10 and ZrGO20 were 4, 18 and 16%, respectively.

The addition of GO leads also to a significant alteration in the total pore volumes and especially in the volume of mesopores. It is worth mentioning that all materials have both a micro and mesoporous nature (Fig. 2C), with the ratio of the micropore to mesopore volumes decreased with the addition of GO (Fig. 2B). While the addition of 1 % GO to ZrOH affected only slightly the volume of the pores, the increase in the pore volume of ZrGO5 was the most pronounced. Its pore volumes are 17, 83 and 52 % higher than V_{mic} , V_{mes} and V_{total} for ZrOH, respectively. For the composites with 10 and 20 % of GO, the increase in the pore volume is less pronounced than that for ZrGO5. The results indicate that 5 % GO is a critical/optimal amount for the development of the high porosity.

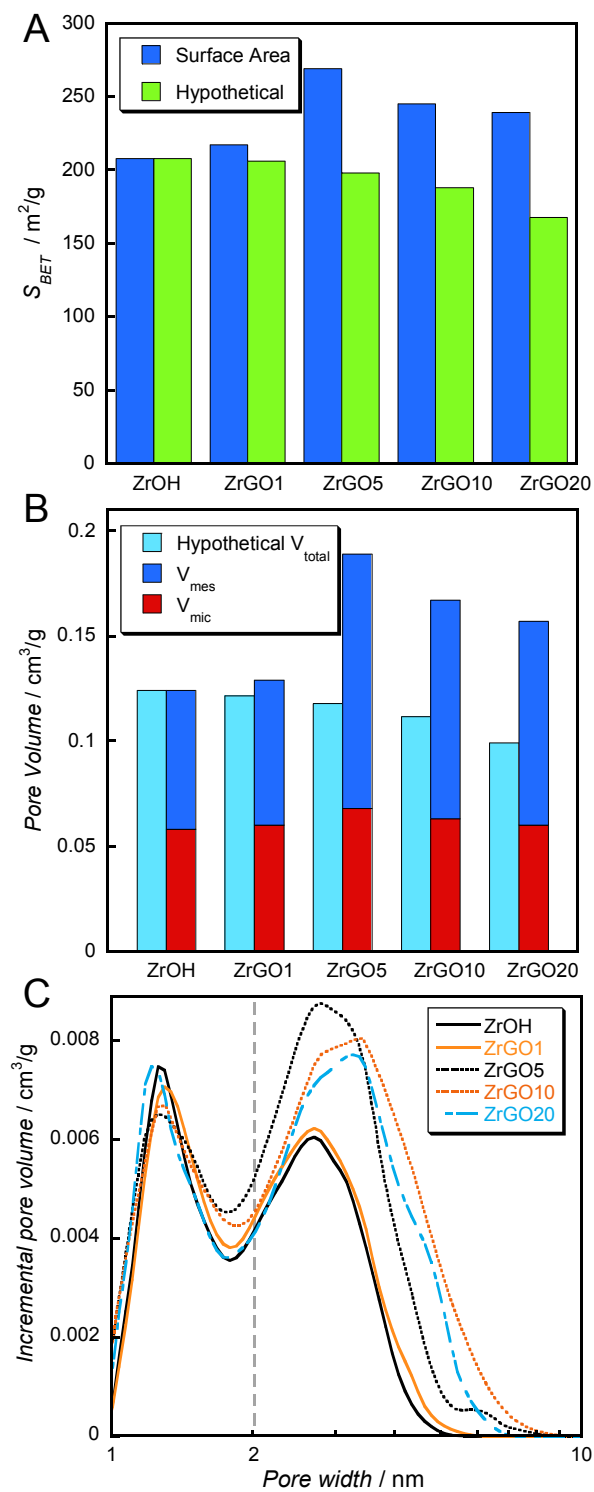


Fig. 1. A) Comparison of the measured and hypothetical surface areas; B) micro and mesopores volumes, and C) pore size distributions.

The SEM images (Fig. 2) show the heterogeneous features of the ZrOH surface. The addition of 1 % GO leads to smaller zirconium hydroxide particles than those in ZrOH. They surround the GO flakes. Further increase in the content of GO leads to an enhance dispersion of the inorganic phase around GO, and encapsulates more GO in the formed particles.

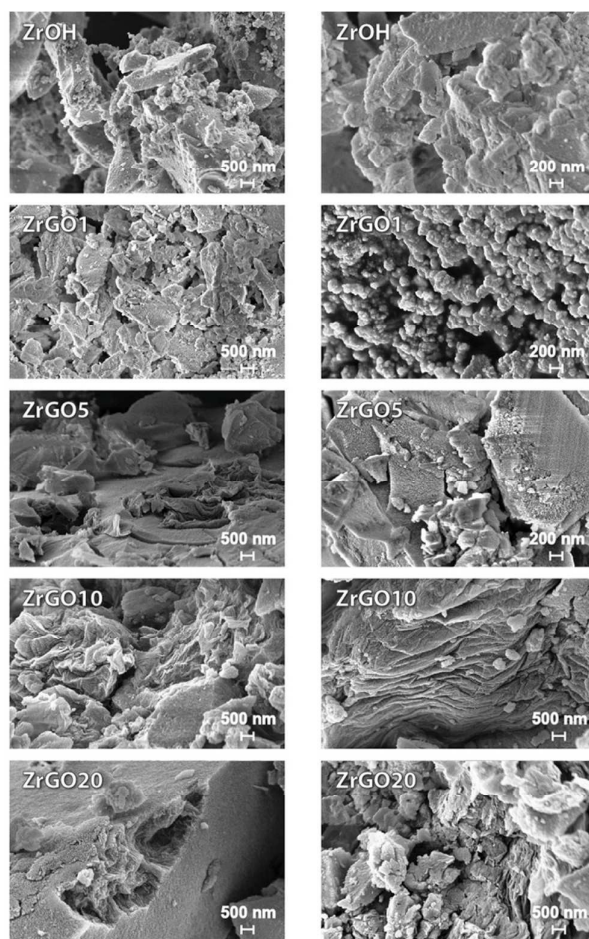


Fig. 2. SEM images of the samples' morphology.

The amount of functional groups on the surface was determined using the potentiometric titration method. For zirconium (hydr)oxide they can be grouped to

two categories: those with pK_a between 7 and 9, and those with pK_a higher than 9. The first ones are linked to oxygen bridging groups and coordinated water, while the second ones- to hydroxyl terminal groups.^{5,9} It was reported that the terminal hydroxyl groups played a key role in the adsorption of CEES vapors on zinc and iron (hydr)oxide.^{31,32} They were also found crucial for the removal of VX nerve agent on $Zr(OH)_4$ ³³ as well as of H_2S on metal (hydr)oxides.^{4,34} Fig. 3 clearly shows that the GO addition leads to an increase in the number of functional groups. The most pronounced increase was found for ZrGO5, which has the highest number of surface acidic species. Compared to ZrOH, the number of groups having pK_a higher than 9 increased 141 % and the number of groups dissociating between 7 and 9 increased 56 %. Interestingly, the composite with 1 % GO has almost the same number of groups as does ZrGO5. A further addition of the carbonaceous phase leads to a decrease in the number of surface groups, however the amount of groups is always than that on ZrOH. It is worth to mention that the synergistic effect of the composite formation on the amount of functional groups on the surface is also seen from the comparison of the measured and hypothetical values calculated assuming a physical mixture. Since the total number of functional groups of GO in the pK_a range 7 to 11 calculated experimentally is 2.009 mmol/g, the measured amounts of functional groups are higher than the hypothetical values by 95, 91, 36 and 1 % for ZrGO1, ZrGO5, ZrGO10 and ZrGO20, respectively.

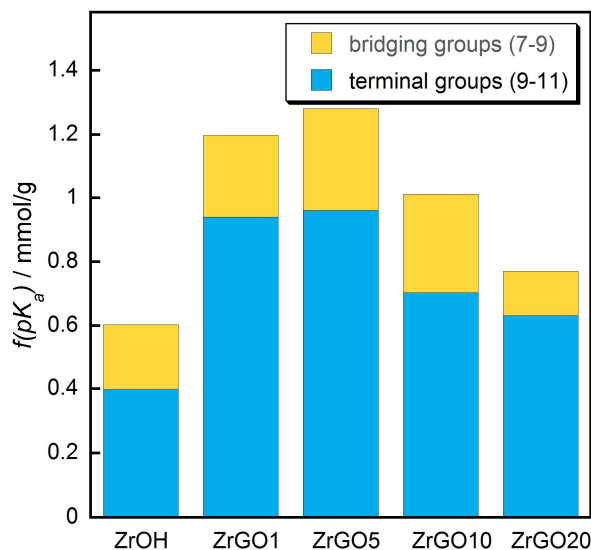


Fig. 3. Amounts of bridging and terminal groups detected from the potentiometric titration experiments.

The above mentioned results indicate that 5 % GO is the optimum amount of the carbonaceous phase resulting in the material with both high porosity and rich surface chemistry. Thus the addition of GO plays an important role in increasing the dispersion and amorphicity of the inorganic phase.

The differential thermal gravimetric (DTG) curves for the initial samples are presented in Fig. 4A. For all samples, a gradual weight loss from a low temperature up to 400 °C is observed. Until 120 °C, it can be linked to the removal of physically adsorbed water and the coordinated water ligands. Above this temperature, the dehydroxylation of the complex hydroxide structure of zirconium hydroxide to the bridged structure takes place (Fig. 4B). The decomposition of the epoxy groups of GO is visible at 190-210 °C^{4,9,35} for the samples with the high content of GO. Sharp and

low intensity peaks between 450 °C and 650 °C are assigned to the formation of metastable tetragonal or monoclinic zirconium oxide.^{5,36}

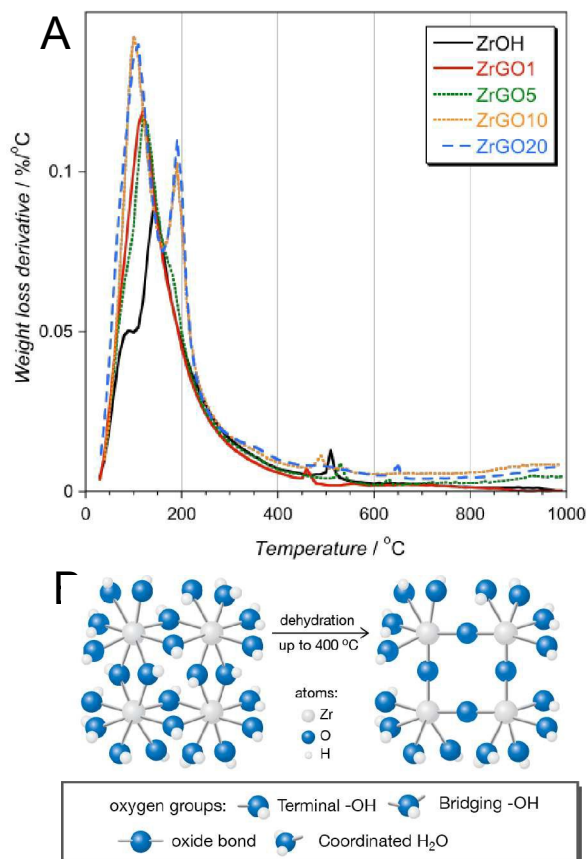


Fig. 4. DTG curves measured in helium for the initial samples (A), and a stereoview of the dehydration of the hydrated zirconium hydroxide (B).

Clearfield et al. first pointed out that the addition of a base to $\text{ZrOCl}_2 \cdot 8\text{H}_2\text{O}$ leads to the formation of a polymeric oxohydroxide with the general formula $[\text{ZrO}_b(\text{OH})_{4-2b} \cdot x\text{H}_2\text{O}]$.^{10,37} This structure (Fig. 4B) consists of four types of oxygen groups. On the outer phase of the structure, there are terminal $-\text{OH}$ groups and coordinated water molecules. In the interior part of the matrix, the Zr atoms are connected via bridging $-\text{OH}$ groups as well as oxide bonds. The existence of both types of hydroxyl groups was also reported by Chitrakar et al. in the case of the $\text{ZrO}(\text{OH})_2 \cdot (\text{NaO})_{0.005} \cdot 1.5\text{H}_2\text{O}$

and by Huang et al. for the $\text{Zr}(\text{OH})_4$.^{10,36} Zirconium hydroxide reported in the literature revealed a broad weight loss up to 400 °C, which was linked to the dehydration. Assuming the existence of pure $\text{Zr}(\text{OH})_4$, its thermal transformation to ZrO_2 should lead to a 22.6 % weight loss. In our case, the weight loss of the unmodified ZrOH was 16.7 % up to 400 °C. Based on this, we can assume that our materials have the random amorphous structure of hydrate zirconium (hydr)oxide instead of zirconium oxide. The terminal –OH groups are proved to be more active towards organic molecules and, owing to their position in the lattice, they may interact faster with the CEES, while the bridging groups are less active and will interact slower, since the diffusion into the lattice requires a longer time.¹⁰

All studied samples were tested for adsorption of 2-chloroethyl ethyl sulfide vapors (CEES) in a close system.^{17,31,38} The weight gains measured are compared in Fig. 5. Owing to the negligible adsorption capacity of GO (7 mg/g), the hypothetical values for the adsorption capacity would be expected to decrease with the increasing GO content. On the contrary, all the GO modified samples reveal the adsorption capacity greater than that for the ZrOH sample, showing a significant synergetic effect of the composite formation. The highest capacity is found for ZrGO5 and it is 67 % higher than that of ZrOH and 75 % higher than that calculated for the hypothetical physical mixture of the composite components. The amounts adsorbed on ZrGO1, ZrGO10 and ZrGO20 were higher than that of ZrOH by 9, 39 and 28 %, respectively.

For the sake of comparison, the reported previously CEES vapor adsorption capacities measured at the same conditions on hydrous ferric oxide and Zn hydroxide (FeO and ZnOH) and their composites with 10 % wt GO (ZnOHGO and FeOGO) are also

displayed in Fig. 5A.^{29,32} The weight uptakes on the composites of GO with Zn and Fe (hydr)oxides were also significantly higher than those for the hydroxides without the carbonaceous phase. The reported in the literature vapor adsorption capacities of coconut shell based activated carbon with a high surface area (1250 m²/g) and its composite with NaOH and CrO₃,³⁸ of porous MgO and its composites with Fe₂O₃ or SiO₂ as well as carbon-coated magnesium oxide (MgO/C-1) are presented in Table 1.^{39,40} Notably, ZrGO5 showed the best performance among all materials addressed so far as the CEES vapor adsorbents. The dependence of the CEES adsorption capacity after 24 h exposure on the surface area, on the number of terminal hydroxyl groups and on mesopore volume is presented in Fig. 5B. Linear correlations suggest that these factors play important roles in the adsorption process.

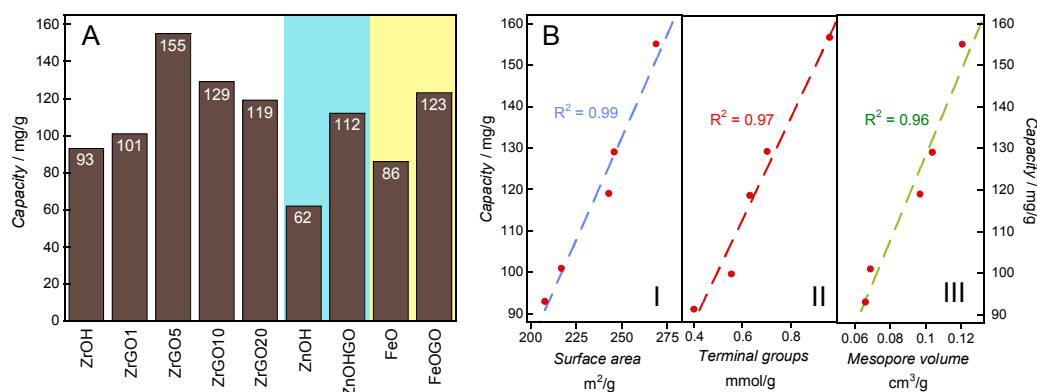


Fig. 5. (A) Adsorption capacities of the Zr-, Zn- and Fe (hydr)oxides and their composites with graphite oxide. (B) Dependence of the amount adsorbed on the surface area (I), terminal groups (II) and the mesopore volume (III) for 24 hours of CEES exposure.

Table 1. Reported Weight uptakes after vapor adsorption of CEES. The results under static conditions are after 24 hours of adsorption.

Materials	Adsorption method	Capacity (mg/g)	ref
Commercial ZnO	Closed adsorption system	29	31
Zn(OH) ₂	Closed adsorption system	62	30
Zn(OH) ₂ /GO composite	Closed adsorption system	112	30
FeO(OH)	Closed adsorption system	86	32
FeO(OH)/GO composite	Closed adsorption system	123	32
MgO	breakthrough	36	39
MgO Fe ₂ O ₃ composite	breakthrough	31	39
MgO SiO ₂ composite	breakthrough	49	39
MgO/C-1 composite	breakthrough	35	40
Activated carbon	Closed adsorption system	< 80	38
Activated carbon/NaOH/CrO ₃	Closed adsorption system	< 80	38
Zr(OH) ₄	Closed adsorption system	93	This study
Zr(OH) ₄ /GO composite	Closed adsorption system	155	This study

FTIR spectra were used to evaluate the changes in surface chemistry after the adsorption of CEES (Fig. 6). The characteristic vibrations for zirconium hydroxide appear at 1590, 1390 and 854 cm⁻¹. The broad band at 1590 cm⁻¹ is attributed to -OH groups of water molecules and at 1390 cm⁻¹ to O-H vibration from Zr-OH.^{5,9} The small band at 854 cm⁻¹ is assigned to the lattice vibration of a Zr-O bond. For graphite oxide, the stretching vibration of C-O bonds from carboxylic groups, bending vibration of O-H from hydroxyl/phenol groups, and O-H vibration of water appear at 1050, 1390 and 1630 cm⁻¹, respectively. The band at 990 cm⁻¹ corresponds to epoxy/peroxide groups, while the band at 1730 cm⁻¹ is characteristic of a C=O stretching vibration in carboxylic acids and the band at 1228 cm⁻¹ might be related to C-O vibrations in epoxides. The vibrations of oxygen groups from graphite oxide are not

visible for the composites with the low GO content (1, 5 and 10%) owing to the involvement of these groups in the formation of the composites. For the sample with 20 % GO, only one broad peak at 990 cm^{-1} appears that corresponds to the vibration of epoxy/peroxide groups. The characteristics bands of zirconium hydroxide are visible for all samples. The exhausted samples are referred to with letter E added to their names. After the CEES vapor adsorption, the intensities of the bands at 850, 1390, and 1590 decrease, indicating that the -OH groups and the water molecules participate in the reactive adsorption.

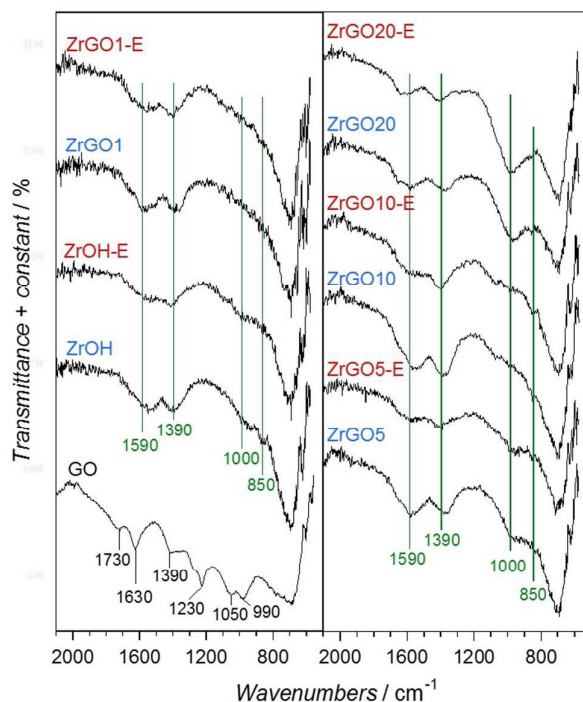


Fig. 6. FTIR spectra of the initial and exhausted (-E) samples.

The differential thermal gravimetric (DTG) curves for the exhausted samples are presented in Fig. 7. The formation of the new compounds after the adsorption is evident since four new peaks appear at 110, 170, 270, and $300\text{ }^{\circ}\text{C}$ with various

intensities for all exhausted materials. We refer to them as Peak 1, 2, 3 and 4, respectively. Mass spectrometry of the exhaust gases/vapors was carried out simultaneously with the TA analysis in order to determine the origin of these new peaks. The assignment discussed below is based on the detected m/z fragments. The MS thermal profiles for ZrOH are collected in Fig. 8. Nomenclature, abbreviations and details on the detected compounds are collected in Table 2.

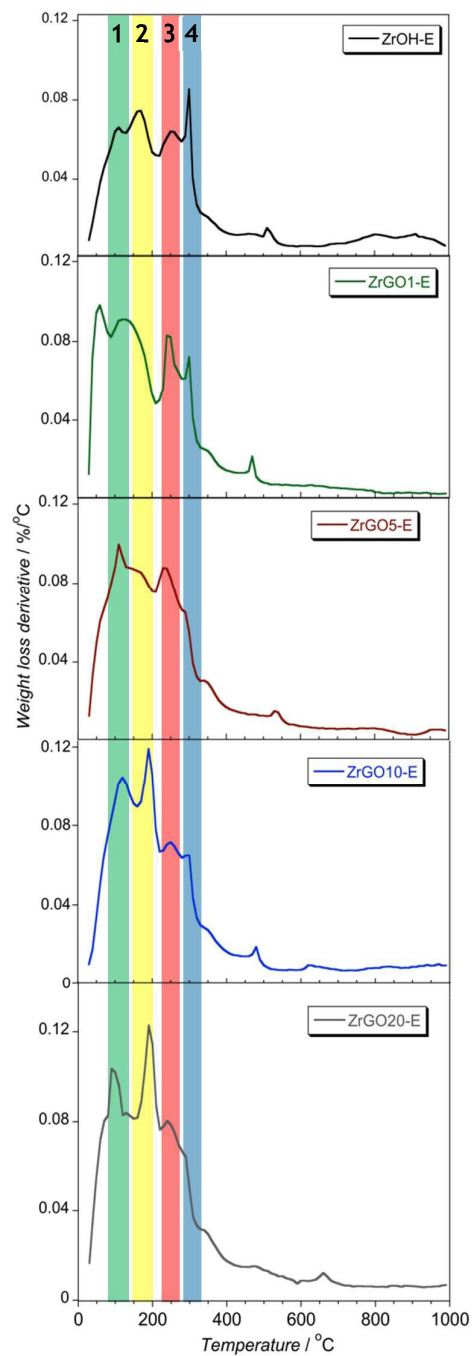


Fig. 7. DTG curves in helium for the exhausted samples.

Table 2. Details on the detected compounds on the surface and in the headspace.

Name	Chemical formula	Abbreviation	Characteristic mass –to-charge ratio (m/z)
2-chloroethyl ethyl sulfide	CH ₃ CH ₂ SCH ₂ CH ₂ Cl	CEES	124, 109, 90, 75, 61, 47
2-hydroxyethyl ethyl sulfide	CH ₃ CH ₂ SCH ₂ CH ₂ OH	HEES	106, 90, 75, 61, 47
1,2-bis(ethylthio) ethane	CH ₃ CH ₂ SCH ₂ CH ₂ SCH ₂ CH ₃	BETE	150, 122, 90, 75, 61, 47
Ethyl ethyl sulfide	CH ₃ CH ₂ SCH ₂ CH ₃	EES	90, 75, 61, 47
Ethyl vinyl sulfide	CH ₃ CH ₂ SCH=CH ₂	EVS	88, 73, 59, 45
Diethyl disulfide	CH ₃ CH ₂ SSCH ₂ CH ₃	DEDS	122, 94, 66, 60, 47, 45
1,4-butanedithiol	SHCH ₂ CH ₂ CH ₂ CH ₂ SH	BDT	122, 88, 73, 60, 55, 47

Based on the m/z thermal profiles, Peak 1 at the DTG with a maximum at 110 °C, can be assigned to CEES (m/z: 90, 75, 61, 47) and to the compounds with identical series of main-intense m/z signals. The latter species include BETE, HEES and/or saturated sulfides such as EES. Moreover, it can be also assigned to EVS (m/z: 88, 73, 59, 45) and DETS (m/z: 66, 60, 47). Peak 2 with a maximum at 170 °C is related to the dehydroxylation, since only the profile of the OH (m/z: 17) gives signal at this temperature. The lower intensity of this peak and the higher temperature of the decomposition, compared to that for the initial sample, suggest that the hydroxide groups are involved in the adsorption/degradation of CWA and they are stabilized by interactions, such as polar or hydrogen bonds, with the organic molecules. Moreover, for the composites with higher amount of GO (ZrGO10 and ZrGO20), the decomposition of GO in the same temperature range contributes to an increase in the intensity of the peak. Peak 3 (maximum at 270 °C) likely represents DEDS and BDT, since the m/z 55 which is characteristic for the later compound appears only at this temperature. Peak 4 at 300 °C can be linked to CEES, HEES, BETE, EVS and EES. The existence of two decomposition temperatures for the same compound is linked to

the adsorption at sites of two different energies.⁴¹ The first one, at a lower temperature, represents weakly adsorbed molecules, likely via polar forces on the external surface and/or in the mesopores and the second one - the removal of strongly adsorbed molecules in the micropores or those hydrogen bonded to the OH groups. The same trends for the removal of CEES and EVS were found for the adsorption of CEES on iron and zinc (hydr)oxides.^{17,31}

For ZrOH, the evolution of the m/z signals corresponding to Cl (m/z: 35) supports the removal of CEES at two different temperatures seen by two maxima at 100 and 300 °C. Moreover, a small maximum at temperature lower than 60 °C is linked to the formation of small molecules containing chloride and a stable signal above 600 °C can be assigned to the decomposition of the Zr-Cl bonds. Finally, the evolution of the m/z signals of SO₂ (m/z: 64), CH₃ (m/z:15) and carbon (m/z: 12) further supports the decomposition of a variety of compounds at the aforementioned temperatures. The acquired m/z thermal profiles for the composites show the same origin of the new peaks. Since many compounds can be formed upon heating during the TA analysis, this method does not provide enough evidence for the mechanism and the progress of the adsorption process.

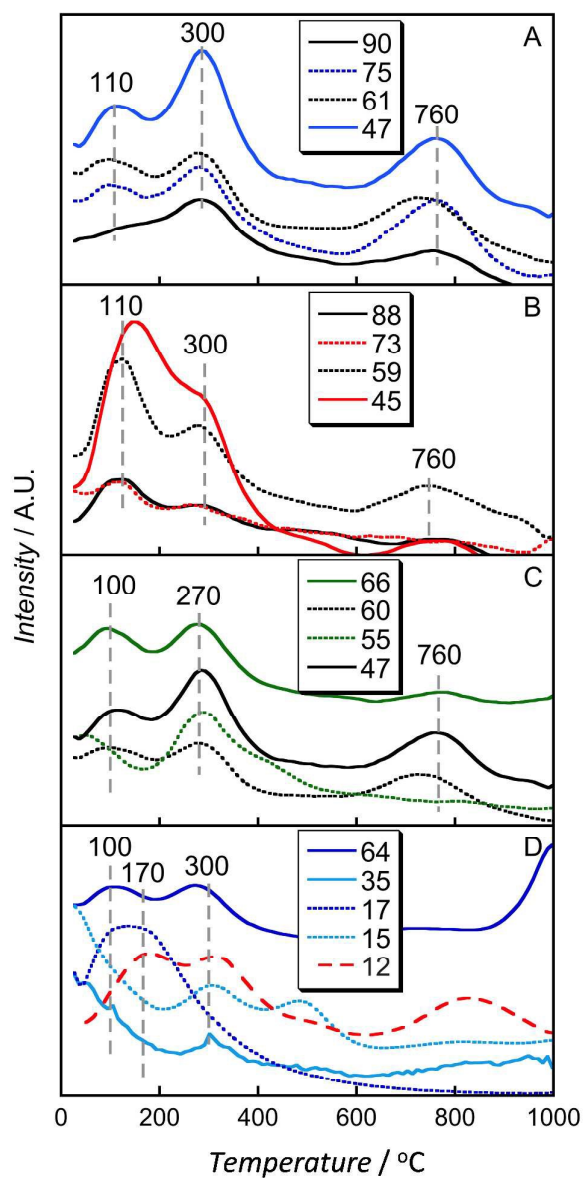


Fig. 8. m/z thermal profiles (in helium) of exhausted ZrOH for the fragments related to CEES, BETE, HEES and/or EES (A), EVS (B), DEDS and/or BDT (C) and to SO_2 (m/z : 64), Cl (m/z : 35), $-\text{OH}$ (m/z : 17), CH_3^+ (m/z : 15) and C (m/z : 12).

In order to determine the maximum weight uptake and to analyze the progress of adsorption, different CEES exposure times were studied (Fig. 9). Since ZrGO5 showed the greatest performance for CEES adsorption after 24 and 48 hours among all others composites, this sample along with ZrOH were chosen to study the extent of the adsorption in more detail. ZrOH reached the maximum weight uptake after 36 hours (106 ± 6.2 mg/g). For ZrGO5, the maximum weight uptake was revealed after 48h with almost twice more weight increase (205 ± 8.3 mg/g) than that on ZrOH. For the other composites the weight increases after 24 and 48 hour of CEES exposure are also included in Fig. 9. The results show that the graphene phase enhanced the amount of CEES adsorbed and/or the amount of degradation products adsorbed on the surface. Furthermore, the correlations of the maximum capacity (at 48 hours) with the surface area, mesopore volume and number of the numbers terminal groups showed linear trends, with R^2 values 0.97, 0.96 and 0.97, respectively. The results indicate that both chemical and physical properties of the materials play a key role on the adsorption performance, suggesting that chemical and physical interactions are involved in the reactive adsorption process. The increased porosity and the amount of the surface groups of ZrGO5 result in reaching the high adsorption capacity quickly. It has to be mentioned here that long adsorption times are only apparent since a low vapor pressure of CEES causes that a considerable length of time is required for its evaporation. Prasad et al. reported that the maximum weight uptake of mustard gas on activated carbon (with surface area 1250 m²/g) was reached after 576 hours (24 days).³⁸

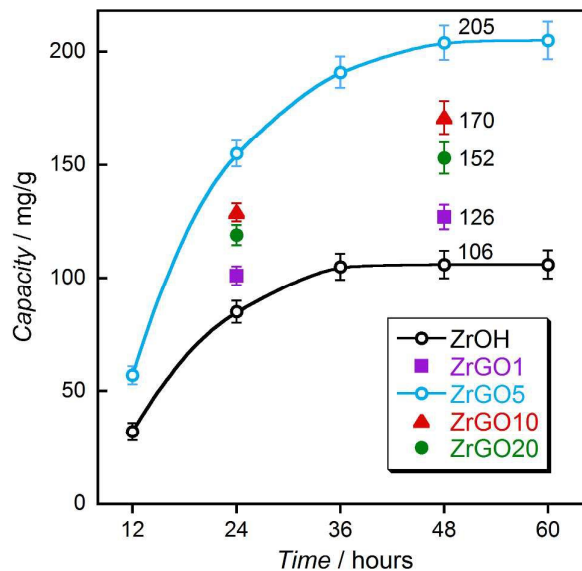


Fig. 9. Weight uptakes/adsorption capacities measured up to 60 hours of CEES exposure.

An increase in the exposure time to 48 hours increased the amount of CEES adsorbed and/or the amount of its decomposition products adsorbed. It is likely due to slow transformations, which take place on the surface of the materials, or the limitation of the time needed for the evaporation of the CEES. Even though the adsorption performance can be evaluated by the measured weight increase, the latter cannot provide a sufficient sole evidence about the activities and the mechanism of the interactions. Therefore, to study in detail the interactions and to throw light on the products of the surface reactions, the headspace of the closed adsorption system and the extracts from the exhausted materials were analyzed by GC-MS. As mentioned above, we focus on ZrGO5 and ZrOH. For both ZrOH and ZrGO5, CEES in the headspace was detected at the elution time of 3.3 min, EVS- at 1.8 min, and BETE- at 4.8 min. The chromatograms after 48 hours are presented in Fig. 10A. The intense peak at 3.3 min indicates that marked amount of CEES vapors is still present in the

reaction vessel even after 48 hours. The low intensities of the peaks representing EVS and BETE are due to the saturation of the headspace with CEES.

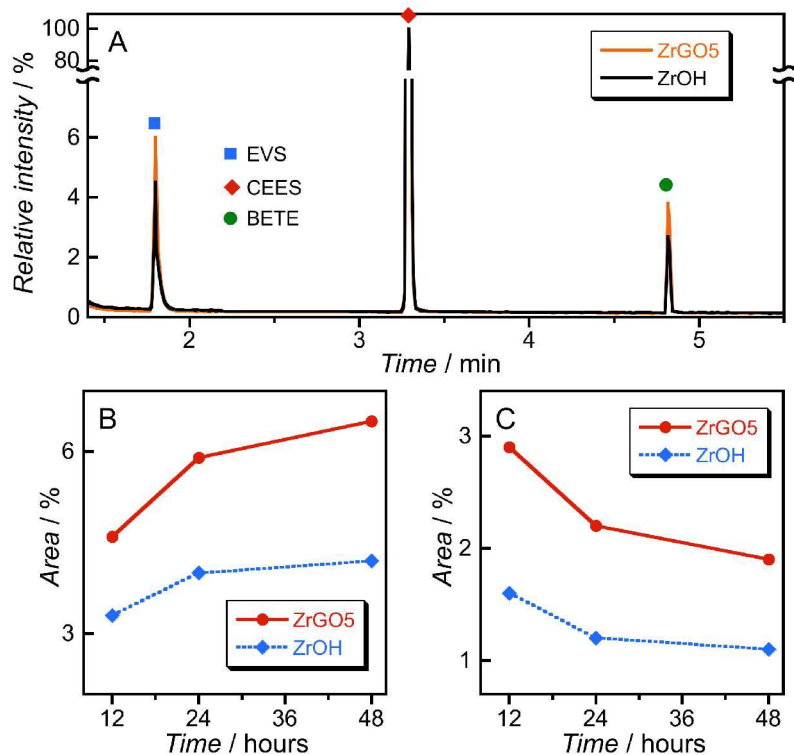
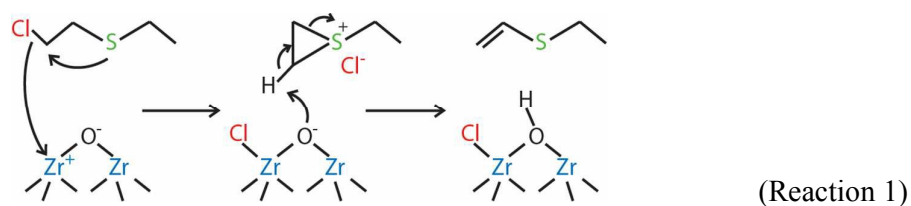


Fig. 10. Chromatograms of the headspace for ZrOH and ZrGO5 after 48 hours of CEES exposure (A) and dependence of the area of the chromatographic peak (analysis of the headspace) of EVS (B) and BETE (C) on the exposure time.

The trends in the concentration of EVS and BETE in the headspace (peak areas) with the progress of adsorption are presented in Fig. 10B and 10C. The results suggest that various interactions/reactions between CEES and the surface of the samples take place simultaneously. The continuous increase in the amount of EVS detected in the headspace supports the TA-MS results. This indicates that the degradation of CEES

leads mainly to the dehydrohalogenation product (Reaction 1). CEES can be transformed to a transient cyclic sulfonium cation by an intermolecular cyclization process. Sulfur atom acts as a nucleophile and attacks the electrophilic carbon to which the chloride is bonded. Afterwards, via a bimolecular elimination (E2) reaction, a labile hydrogen from the cyclic cation transfers to a negatively charged lattice oxygen of the zirconium phase, which acts as a Lewis base. The cleavage of the C-Cl bond in the first step of this elimination pathway is promoted by the Lewis acidic Zr(IV) centers. The analogous degradation pathway was reported for the adsorption of CEES or HD on aluminium oxide, zinc hydroxide, and iron oxyhydroxide.^{17,31,42} The thermal profile of m/z 35 shows a strong signal at the temperature of ZrCl_4 decomposition (330 °C) owing to the bonds between the chlorine atoms and the inorganic matrix as a result of the intermolecular cyclization process.



Dehydrohalogenation of CEES to EVS by an intermediate cyclic sulfonium cation.

The trend in the BETE concentration showed an opposite trend compared to that for EVS. The downswing of the concentration of BETE in the headspace is linked to both its limited formation and a simultaneous strong retention on the surface. The mechanism of the BETE formation includes the cleavage of S-C bond and the creation of a new S-C bond between two distinct molecules. Alkoxy species on the surface react with sulfonium cations, resulting to the formation of BETE and $-\text{OCH}_2\text{CH}_3$ groups. The involvement of the oxygen containing groups in the formation

of the alkoxy species is supported by the FTIR spectra, in which a decrease in intensity of the bands assigned to the $-OH$ was found. Verma et al. reported the formation of EVS as well as of alkoxy species after the interaction of CEES with the isolated hydroxyl groups on ZrO_2 or WO_3 nanoparticles.^{43,44}

The aforementioned pathways require the adsorption of CEES on the surface as a first step. As it was suggested from the TA analysis, there are two diverse adsorption centers with different energies for both CEES and EVS adsorption. The lower energetically adsorption process likely includes the polar interaction of $S^{\delta-}$ with the $Zr^{\delta+}$.^{17,45} Stronger adsorption can be due to the formation of hydrogen bonds between the OH groups of the materials and both S and Cl moieties of the organic molecules. Panayotov and Yates studied in details the adsorption of CEES on a high surface area TiO_2-SiO_2 mixed oxide and they found that hydrogen bonding of this molecule to Si-OH groups occurs through both Cl and S moieties⁴⁶. The removal of the adsorbed molecules at low temperature (110 °C) in the TA-MS analysis is linked to the weak interactions and at higher temperature (300 °C) - to the hydrogen bonding interactions.

The analysis of the surface extracts by GC-MS revealed the existence of both CEES and BETE. It is worth to mention that the signal related to BETE has higher intensity in the chromatograms of the extracts than those of the headspace. The areas corresponding to BETE consist of 16-20 % of the total areas of all detected compounds, while these values were in the range of 1 to 3 % from the analysis of the headspace. HEES, disulfides like DEDS and BDT, or any oxidation product such as sulfoxides and sulfones were not detected either in the headspace or in the extracts.

The possible detection of some of them from the TA-MS analysis can be due to the thermal transformation during the analysis and the involvement of the released oxygen in their formation. Finally, the higher concentrations of BETE in the extracts of the composites than in that of pristine ZrOH further support the fact that the addition of GO leads to a significant increase of the adsorption performance and in the selective catalytic transformation of CEES to EVS and BETE. It is due to the successful improvement of the active surface features and chemical heterogeneity of the composites. The increased dispersion of the hydroxyl groups and the developed porosity play the key roles in the detoxification process.

All the above-mentioned interactions of CEES and of its degradation byproducts with the samples' surfaces are presented in Fig. 11. The amorphous zirconium hydroxide phase acts as a reactive adsorbent, since it physically adsorbs the organic molecules and catalytically transforms CEES to the dehydrohalogenation product, EVS, and to the polymerization product, BETE.

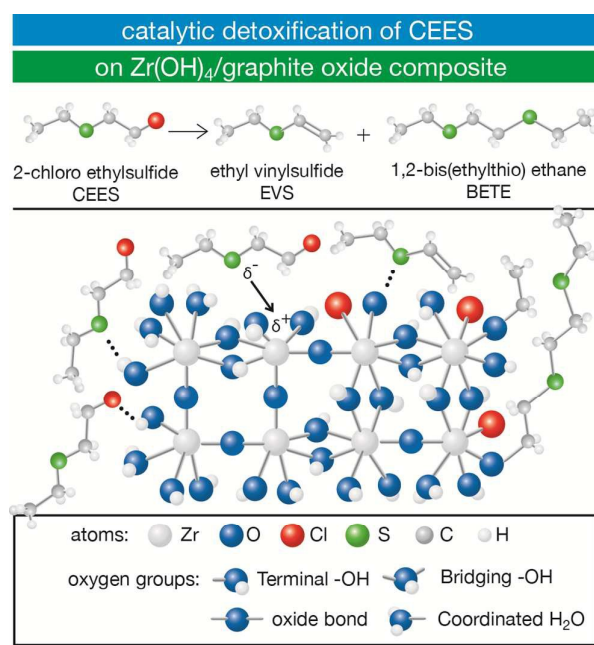


Fig. 11. Proposed reactions scheme of CEES reactive adsorption mechanism.

Conclusions

The results presented in this paper show for the first time that zirconium (hydr)oxide and its composites with graphite oxide can be used as reactive adsorbents of the mustard gas surrogate, 2-Chloroethyl ethyl sulfide (CEES), vapors. The aqueous synthetic route leads to the materials with an amorphous nature, various levels of complexity, a relatively high surface area and a high density of active hydroxyl group. The addition of the carbonaceous phase resulted in an increased degree of the chemical and structural heterogeneity. The most pronounced increases in the surface area (+ 141 %) and in the number of terminal hydroxyl groups (+ 67 %) compared to the unmodified sample were found for the composite with 5 % GO (ZrGO5).

Notably, the pristine zirconium (hydr)oxide presented the higher weight uptake than those reported in the literature for hydrous ferric oxide and zinc hydroxide (at the same conditions for 24 hours). The weight uptake capability significantly improved with the addition of GO, with 5 % as the optimum amount. ZrGO5 showed the best adsorption performance (155 mg/g after 24 hours and 205 mg/g after 48 hours). The results indicate the paramount role of the porosity and surface chemistry in the reactive adsorption process of CEES.

Two general adsorption pathways were proposed based on the collected results. The first one is the retention of the organic molecules by physical forces and the second is the catalytic and selective transformation of CEES to ethyl vinyl sulfide by dehydrohalogenation and to 1,2-bis(ethylthio) ethane by polymerization. The degradation yields on the composites with carbonaceous phase were also higher than that on the unmodified sample.

Experimental

Materials

Zirconium chloride (ZrCl_4 , 98%, anhydrous, Acros Organics), sodium hydroxide (NaOH , >99%, ACS grade, Amresco), 2-Chloroethyl ethyl sulfide (CEES, 98%, Sigma-Aldrich), and deionized water was used. Commercial graphite (Sigma-Aldrich) was oxidized under Hummers method (details of GO preparation are presented elsewhere).⁴⁷ All the materials were synthesized following a precipitation procedure at room temperature.^{4,31}

Sample Synthesis

The composites of zirconium (hydr)oxide/graphite oxide were prepared using a one-pot in situ precipitation method by dispersing GO powder (1, 5, 10 and 20 wt % of the final mass of the material) in 2 L of a sodium hydroxide solution (0.05 M). The suspension was maintained under vigorous stirring for 2 hours. Then, the stoichiometric amount of zirconium chloride (0.5 L, 0.05 M) was added with a rate of 0.6 mL/minute. The obtained precipitate was filtered and then washed with deionized water until no traces of chloride ions were found. Finally, a separated gel phase was dried at 60 °C for 48 h. The composites obtained with 1, 5%, 10% and 20% of GO are referred to as ZrGO1, ZrGO5, ZrGO10 and ZrGO20. Pristine zirconium hydroxide (ZrOH) was prepared in the same way, but without the addition of GO.

CEES reactive adsorption measurements. The reactive adsorption of CEES was studied in batch experiments. Two 1 mL reaction vessels were placed in a 22 mL glass vial. In the first vessel, 20 mg of sample was inserted before the addition of CEES and the vial was tightly capped with a septum, resulting in a closed system

(Fig. S2). Through the septum, 40 μL of as received liquid CEES was injected into the second reaction vessel. The vessels were kept in ambient conditions from 24 to 144 hours, depending on the target experiment. The vapor phases from the headspace of the glass vials were sampled with a syringe at specified time periods and injected into the GC-MS. Then, the containers were opened to equilibrate the adsorbents for 1 h under ambient conditions with the exception of ensuring a lack of moisture in the environment. Lastly, reaction vessels containing the samples were weighed and any change in weight was recorded. Exhausted samples after exposure to CEES are referred to with letter “E”.

Methods

FT-IR Spectroscopy. The Fourier transform infrared (FTIR) spectra were obtained in a Nicolet Magna-IR 830 spectrometer using the attenuated total reflectance (ATR) method. The spectrum was generated and collected 64 times in the wave range between 4000 and 400 cm^{-1} and corrected for the background noise.

X-Ray Diffraction (XRD). X-ray Diffraction (XRD) patterns were obtained on a Phillips X’Pert X-ray diffractometer with powder diffraction procedure, using a $\text{CuK}\alpha$ radiation (operated at 40 kV and 40 mA). The diffraction patterns were collected from a 10 to 70 2θ scan.

Simultaneous Thermal Analysis – Mass Spectroscopy (TA-MS).

Thermogravimetric (TG) curves were obtained from a TA Instruments Thermal Analyzer (SDT 2960). The thermo gravimetric and differential thermal curves were obtained under a helium atmosphere at 100 mL / min with heating rate 10 $^{\circ}\text{C}$ per minute from ambient temperature to 1000 $^{\circ}\text{C}$. TG curves were used to determine the derivative thermogravimetric curves (DTG). Simultaneously, gases and vapors

released with an increased temperature were analyzed with a ThermoStar Gas Mass Spectrometer (GSD; Pfeiffer Vacuum). The off-gas collected was scanned with a secondary electron multiplier detector and a Faraday detector. The m/z identified in the MS was correlated in real time with their corresponding releasing temperature and the MS profiles were obtained.

Potentiometric Titration. Potentiometric titration measurements were performed with an automatic titrator (888 Titrand, Metrohm). In a container, 50 mg of the sample and 25 mL NaNO_3 (0.01M) were added and maintained overnight at 25 °C and continuous stirring for equilibrium. Nitrogen (N_2) was used to eliminate the influence of atmospheric CO_2 by saturating the suspension throughout the entire experiment. Starting from the initial pH of the suspended sample, volumetric standard sodium hydroxide (0.1 M) was used as the titrant up till pH 11. The experimental titration curves were transformed into proton binding curves (Q), where Q represents the total number of protonated sites.^{48,49} The pK_a distributions for the species present on the surface were obtained using the SAIEUS procedure.⁴⁹

Adsorption of Nitrogen. Nitrogen isotherms were measured using an ASAP 2020 (Micromeritics) at -196 °C. Samples were outgassed at 120 °C to 10^{-4} Torr before the measurements. The surface area, S_{BET} (Brunauer–Emmet–Teller method was used), the micropore volume, V_{mic} (calculated using the Dubinin–Radushkevich approach) the mesopore volume, V_{mes} , the total pore volume, V_t (calculated from the last point of the isotherms based on the volume of nitrogen adsorbed) was calculated from the isotherms. The volume of mesopores, V_{mes} , represents the difference between the total pore volume and the micropore volume.

Scanning electron microscopy (SEM). The morphology of the catalysts was

observed with a Zeiss Supra 55 VP (accelerating voltage of 5.00 kV) and was performed in situ on the powder samples.

GC-MS analysis. Both the headspace of the reaction containers and the extracts of the exhausted materials were analyzed using a GC-MS QP5050A (Shimadzu). The separation of the compounds was performed in XTI-5 column (5% dephenyl-95% dimethyl polysiloxane) of 30 m length, 0.25 mm internal diameter, and 0.25 μm of liquid film thickness. The GC operation program was as follows: an increase from 50 $^{\circ}\text{C}$ to 100 $^{\circ}\text{C}$ at a rate of 5 deg/min, then the rate was changed to 40 deg/min up to 280 $^{\circ}\text{C}$. Helium was used as a carrier gas. The injection volume, total flow and the split ratio was 40 μL , 17.8 mL and 8, respectively. The mass spectrometer detector was used in an electron impact ionization mode. For the extractions, 20 mg of exhausted material was equilibrated with 5 mL of the extracting agent (acetonitrile) for 5 days. Then, the solution was filtrated and injected for analysis.

Acknowledgements

This work was supported by the ARO (Army Research Office of USA), grant W911NF-13-1-0225 and NSF collaborative CBET Grant No. 1133112. DG is grateful to Dr. Mykola Seredych for the fruitful discussion and Dr. Javier Arcibar-Orozco for the valuable training on GC-MS.

BIBLIOGRAPHY

- 1 T. Marrs, R. Maynard and F. Sidell, *Chemical warfare agents: toxicology and treatment*, Wiley, West Sussex, England, 2nd ed., 2007.
- 2 B. Jang and J. Spivey, *Catal. today*, 2000, 55, 3–10.
- 3 J. E. Mondloch, M. J. Katz, W. C. Isley Iii, P. Ghosh, P. Liao, W. Bury, G. W. Wagner, M. G. Hall, J. B. Decoste, G. W. Peterson, R. Q. Snurr, C. J. Cramer, J. T. Hupp and O. K. Farha, *Nat. Mater.*, 2015, 14, 1-5.
- 4 D. A. Giannakoudakis and T. J. Bandosz, *J. Colloid Interface Sci.*, 2014, 436, 296–305.
- 5 M. Seredych and T. Bandosz, *J. Phys. Chem. C*, 2010, 114, 14552–14560.
- 6 G. W. Peterson and J. A. Rossin, *Ind. Eng. Chem. Res.*, 2012, 51, 2675–2681.
- 7 V. Štengl, T. M. Grygar, F. Opluštil and T. Němec, *J. Hazard. Mater.*, 2011, 192, 1491–1504.
- 8 B. Levasseur, A. M. Ebrahim and T. J. Bandosz, *Langmuir*, 2011, 27, 9379–9386.
- 9 M. Seredych and T. J. Bandosz, *Chem. Eng. J.*, 2011, 166, 1032–1038.
- 10 R. Chitrakar, S. Tezuka, A. Sonoda, K. Sakane, K. Ooi and T. Hirotsu, *J. Colloid Interface Sci.*, 2006, 297, 426–33.
- 11 T. G. Glover, G. W. Peterson, J. B. Decoste and M. A. Browe, *Langmuir*, 2012, 28, 10478–10487.
- 12 L. Kumari, G. H. Du, W. Z. Li, R. S. Vennila, S. K. Saxena and D. Z. Wang, *Ceram. Int.*, 2009, 35, 2401–2408.

- 13 G. W. Peterson, C. J. Karwacki, W. B. Feaver and J. A. Rossin, *Ind. Eng. Chem. Res.*, 2009, 48, 1694–1698.
- 14 G. W. Peterson, J. A. Rossin, C. J. Karwacki and T. G. Glover, *J. Phys. Chem. C*, 2011, 115, 9644-9650.
- 15 A. Mattsson, C. Lejon, V. Štengl, S. Bakardjieva, F. Opluštil, P. O. Andersson and L. Österlund, *Appl. Catal. B Environ.*, 2009, 92, 401–410.
- 16 G. Chuah and S. Jaenicke, *Appl. Catal. A Gen.*, 1997, 163, 261–273.
- 17 J. A. Arcibar-Orozco, S. Panettieri and T. J. Bandosz, *J. Mater. Chem. A*, 2015, 3, 17080–17090.
- 18 J. A. Arcibar-Orozco, D. A. Giannakoudakis and T. J. Bandosz, *Adv. Mater. Interfaces*, 2015, 2, 16.
- 19 C. Petit, J. Burrell and T. J. Bandosz, *Carbon*, 2011, 49, 563–572.
- 20 N. A. Travlou, K. Singh, E. Rodríguez-Castellón and T. J. Bandosz, *J. Mater. Chem. A*, 2015, 3, 11417-11429
- 21 S. Bashkova and T. J. Bandosz, *Microporous Mesoporous Mater.*, 2013, 179, 205–211.
- 22 M. Jurow, V. Manichev, C. Pabon, B. Hageman, Y. Matolina and C. M. Drain, *Inorg. Chem.*, 2013, 52, 10576–10582.
- 23 G. Z. Kyzas, D. N. Bikiaris and E. A. Deliyanni, *Mater. Lett.*, 2014, 128, 46–49.
- 24 N. A. Travlou, G. Z. Kyzas, N. K. Lazaridis and E. A. Deliyanni, *Chem. Eng. J.*, 2013, 217, 256–265.

- 25 A. M. Ebrahim, J. Jagiello and T. J. Bandosz, *J. Mater. Chem. A*, 2015, 3, 8194–8204.
- 26 C. Petit, B. Mendoza and T. J. Bandosz, *Langmuir*, 2010, 26, 15302–15309.
- 27 M. Florent and T. J. Bandosz, *Microporous Mesoporous Mater.*, 2014, 204, 8–14.
- 28 H. S. Song, M. G. Park, E. Croiset, Z. Chen, S. C. Nam, H. J. Ryu and K. B. Yi, *Appl. Surf. Sci.*, 2013, 280, 360–365.
- 29 D. A. Giannakoudakis, J. A. Arcibar-Orozco and T. J. Bandosz, *Appl. Catal. B Environ.*, 2016, 183, 37–46.
- 30 M. Seredych and T. J. Bandosz, *J. Colloid Interface Sci.*, 2008, 324, 25–35.
- 31 D. A. Giannakoudakis, J. A. Arcibar-Orozco and T. J. Bandosz, *Appl. Catal. B Environ.*, 2015, 174, 96–104.
- 32 J. A. Arcibar-Orozco and T. J. Bandosz, *J. Mater. Chem. A*, 2015, 3, 220–231.
- 33 T. J. Bandosz, M. Laskoski, J. Mahle, G. Mogilevsky, G. W. Peterson, J. A. Rossin and G. W. Wagner, *J. Phys. Chem. C*, 2012, 116, 11606–11614.
- 34 J. A. Arcibar-Orozco, R. Wallace, J. K. Mitchell and T. J. Bandosz, *Langmuir*, 2015, 31, 2730–2742.
- 35 N. A. Travlou, G. Z. Kyzas, N. K. Lazaridis and E. A. Deliyanni, *Langmuir*, 2013, 29, 1657–1668.
- 36 C. Huang, Z. Tang and Z. Zhang, *J. Am. Ceram. Soc.*, 2001, 38, 1637–1638.
- 37 A. Clearfield, G.H. Nancollas and R. H. Blessing, in *Ion Exchange and Solvent Extraction*, ed. 1, J. A. Marinsky, Dekker, New York, vol. 5, 1973, pp. 1–120.

- 38 G. K. Prasad, B. Singh and A. Saxena, *AIChE J.*, 2006, 52, 678–682.
- 39 A.-T. Vu, J. Shunbo, K. Ho, C.-H. Lee, *Chem. Eng. J.*, 2015, 269, 82-93
- 40 A.-T. Vu, K. Ho, C.-H. Lee, *Chem. Eng. J.*, 2016, 283, 1234-1243
- 41 J. E. R. Abelard, A. R. Wilmsmeyer, A. C. Edwards, W. O. Gordon, E. D. Davis, C. J. Karwacki, D. Troya and J. R. Morris, *J. Phys. Chem. C*, 2015, 119, 365-372.
- 42 Y. Zafrani, M. Goldvaser, S. Dagan, L. Feldberg, D. Mizrahi, D. Waysbort, E. Gershonov and I. Columbus, *J. Org. Chem.*, 2009, 74, 8464–7.
- 43 M. Verma, R. Chandra and V. K. Gupta, *J. Environ. Chem. Eng.*, 2016, 4, 219-229
- 44 M. Verma, R. Chandra and V. K. Gupta, *J. Colloid Interface Sci.*, 2015, 453, 60-68
- 45 D. B. Mawhinney, J. A. Rossin, K. Gerhart and J. T. Yates, *Langmuir*, 1999, 15, 4789–4795.
- 46 D. Panayotov and J. T. Yates, *J. Phys. Chem. B*, 2003, 107, 10560–10564.
- 47 W. S. Hummers and R. E. Offeman, *J. Am. Chem. Soc.*, 1958, 80, 1339.
- 48 J. Jagiello, *Langmuir*, 1994, 10, 2778–2785.
- 49 J. Jagiello, T. J. Bandosz and J. A. Schwarz, *Carbon*, 1994, 32, 687–691.

Captions to the Tables

Table 1. Reported Weight uptakes after vapor adsorption of CEES. The results under static conditions are after 24 hours of adsorption.

Table 2. Details on the detected compounds on the surface and in the headspace. With bold the m/z based on held the identification of the organic molecules.

Captions of the Figures

Fig. 1. A: Comparison of the measured and hypothetical surface areas; B: micro and mesopores volumes, and C: pore size distributions.

Fig. 2. SEM images of the samples.

Fig. 3. Amounts of bridging and terminal groups detected from the potentiometric titration experiments.

Fig. 4. DTG curves measured in helium for the initial samples (A) and a stereoview of the dehydration of the hydrated zirconium hydroxide (B).

Fig. 5. (A) Adsorption capacities of the Zr, Zn and Fe (hydr)oxides and their composites with graphite oxide. (B) Dependence of the amount adsorbed on the surface area (I), terminal groups (II) and the mesopore volume (III) for 24 hours of exposure.

Fig. 6. FTIR spectra of the initial and exhausted (-E) samples.

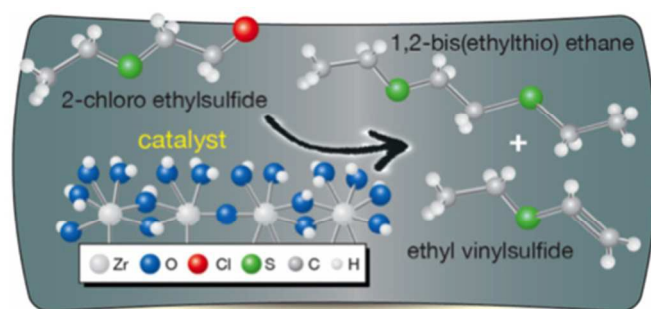
Fig. 7. DTG curves in helium for the exhausted samples.

Fig. 8. MS thermal profiles (in helium) of exhausted ZrOH for the fragments related to CEES, BETE, HEES and/or EES (A), EVS (B), DEDS and/or BDT (C) and to SO₂ (m/z: 64), Cl m/z: (35), -OH (m/z: 17), CH₃⁺ (m/z: 15) and C (m/z: 12).

Fig. 9. Weight uptakes/adsorption capacities measured up to 60 hours of CEES exposure.

Fig. 10. Chromatograms of the headspace for ZrOH and ZrGO5 after 48 hours of CEES exposure (A) and dependence of the area of the chromatographic peak (analysis of the headspace) for EVS (B) and BETE (C) on the exposure time.

Fig. 11. Proposed reactions scheme of CEES reactive adsorption mechanism.



254x190mm (72 x 72 DPI)